physica status solidi a
www.pss-a.com

Investigation of Optical Properties of Pentasodium Trioxoundecafluoro-Trititanate for Optoelectronic Applications

Crispin Munyelele Mbulanga, Rudolph Erasmus, Chinedu Christian Ahia, Hippolyte Nyengeri, Donate Harerimana, Kevin Sadock Niyomugavyi, Edson Leroy Meyer, and Johannes Reinhardt Botha*

A successful application of the Kubelka–Munk model, modified Kubelka–Munk model and unified methodology for estimating the bandgap in semiconducting materials to the analysis of diffuse reflectance spectra for pentasodium trioxoundecafluoro-trititanate ($Na_5(Ti_3O_3F_{11})$) plates grown using a hydrothermal method is reported. The steps involved in interpreting the Kubelka–Munk $F(R)$ function and using it for bandgap determination are presented. Bandgap energy (E_g) calculations are performed after establishing, through an extensive literature review, that (i) values can be obtained by extrapolating a linear fit of the Tauc diagram to zero–using the photon energy axis as the abscissa–for a sample that exhibits negligible absorption of gaps in the sub-bands, but (ii) if absorption of gaps in the sub-bands is observed in the Tauc diagram, a linear fit of the Tauc diagram can be performed as in the method described in (i). In addition, another linear line fit is added and used as a new abscissa to replace the photon energy axis used in point (ii). It is established that pentasodium trioxoundecafluoro-trititanate is a wide-bandgap material, with bandgap energies of 3.70 eV ($p = 1/2$) and 4.0 eV ($p = 2$), respectively.

1. Introduction

Diffuse reflectance spectroscopy represents a valuable and efficacious approach to material characterization, offering non-destructive investigation with high sensitivity. The adaptability of this technique to different wavelengths, including the visible, near-infrared, and mid-infrared regions, has enhanced its usefulness. This has facilitated the application of the technique across a range of disciplines, rendering it a valuable tool in both research and industry. Most importantly, diffuse reflectance spectroscopy is a reliable technique for analyzing the optical absorption characteristics of materials that are problematic to investigate using other traditional transmission spectroscopy procedures. This enables insights to be gained into the electronic and vibrational structures of samples of interest.

The utilization of diffuse reflectance characterization as a technique of choice to investigate the optical properties of $Na_5(Ti_3O_3F_{11})$ can reveal intriguing properties of the material, including thermal stability, structural integrity, and electrical activities. A procedure based on the principles of diffuse reflectance spectroscopy has been proposed[1] as an appropriate technique for characterizing the redox properties of various semiconductor materials. A suitable set of coefficients characteristic of individual ions was clearly established for each semiconductor material using this procedure. Similarly, diffuse reflectance infrared Fourier transform spectroscopy has been demonstrated[2] to be an effective

C. M. Mbulanga
Department of Physics and Applied Sciences
Université Pédagogique de Kananga
P.O Box 282/Kananga, Kananga, Democratic Republic of Congo

C. M. Mbulanga, J. R. Botha
Department of Physics
Nelson Mandela University
P.O Box 77000, Port Elizabeth 6031, South Africa

The ORCID identification number(s) for the author(s) of this article can be found under https://doi.org/10.1002/pssa.202400521.

DOI: 10.1002/pssa.202400521

C. M. Mbulanga, H. Nyengeri, D. Harerimana, K. S. Niyomugavyi
Department of Physics
Université du Burundi
P.O Box 1550, Bujumbura, Burundi

R. Erasmus
School of Physics and Microscopy and Microanalysis Unit
University of the Witwatersrand, WITS
Private Bag 3, Johannesburg 2050, South Africa

C. C. Ahia, E. L. Meyer
Institute of Technology
University of Fort Hare
Private Bag X1314, Alice 5700, South Africa
E-mail: achinedu@ufh.ac.za

technique for the evaluation of incipient heat damage in carbon-fiber-reinforced polymer composites and for the monitoring of degradation mechanisms. A systematic study employing UV-Vis diffuse reflectance spectroscopy has been conducted to examine the impact of the evaluation method on the measured bandgap for a diverse array of photocatalytically active materials, including metal sulfides, $BiVO_4$, niobates, and TiO_2. The studies provided significant insight into the material dependence of diffuse reflectance spectroscopy estimation approaches,[3] along with suggestions for further research. Another significant study included the analysis of the optical bandgap of inorganic compounds such as SnO_2[3] and their sensing mechanisms[4] using diffuse reflectance spectroscopy. These studies, in conjunction with numerous others, have played an instrumental role in substantiating the efficacy of diffuse reflectance spectroscopy in material characterization. Furthermore, Bock et al.[5] put forth an integrated instructional framework for characterizing the absorption and emission properties of pure, dielectric (nano-) powders utilizing diffuse reflectance spectroscopy. The authors demonstrated an appropriate technique for preparing samples, which ensures that their surface acts as a Lambertian scatterer while light transmission through the sample is insignificant. It was demonstrated that this procedure is applicable to the specific case of powders that can be compressed into thick, non-translucent pellets, which is the case of pentasodium trioxoundecafluoro-trititanate powder. Hence, embedding the pentasodium trioxoundecafluoro-trititanate powders within an appropriate host matrix during sample preparation is not a prerequisite for measurements.

In light of the aforementioned discussion, there is a well-established approach for deriving optical parameters from diffuse reflectance spectroscopic data. This methodology enables the quantification of diffuse reflection in inhomogeneous materials and the spectroscopic analysis of materials. This model was developed by Kubelka and Munk to address the inverse problem of acquiring information regarding scattering and absorption from reflected light. Furthermore, it can be employed as a platform for elucidating diffuse reflection in semi-infinite samples, such as materials deposited on substrates. Additionally, the versatility of employing the Kubelka–Munk function in correlating reflectance with absorbance and scattering coefficients can be leveraged to obtain insights into a material's electronic structure and optical properties through the analysis of absorbance spectra.[6] Also, the practical semi-infinite length of the samples to which the Kubelka–Munk model can be applied to, has been estimated to be between 1 and 3 mm.[7]

As detailed in ref. [8], we have devised and proposed a novel approach for synthesizing epitaxial pentasodium trioxoundecafluoro-trititanate ($Na_5(Ti_3O_3F_{11})$) with a plate-like morphology on fluorine-doped tin oxide-coated glass substrates (FTO). This structural type is adopted by a number of fluorides, oxides, and oxyfluorides whose general formula is $A_5M_3X_{14}$ ($X = O_iF_{14-i}$, $i = 0...14$). These materials are known to serve as highly effective host networks for phosphors utilized in a diverse array of applications. To cite a few examples, fluorinated materials can be employed as carriers for laser action or as phosphors for lamps.[9–11] Their high optical transparency and low phonon energy contribute to the significant interest in their use as host materials for luminescent centers, such as rare-earth ions. In our recent publication,[12] we examined the structural and chemical properties of pentasodium trioxoundecafluoro-trititanate as a function of temperature, in preparation for subsequent studies pertinent to the intended applications. In particular, the aforementioned studies[12] utilized temperature-dependent Raman spectroscopy to examine vibrational modes and ascertain the thermal stability of $Na_5(Ti_3O_3F_{11})$. However, further characterization is required for our system, $(Na_5(Ti_3O_3F_{11}))$/FTO/glass, to be considered for the aforementioned applications. As we consider the potential use of $Na_5(Ti_3O_3F_{11})$ as phosphors for lamps or for persistent luminescence hosts, it is essential to conduct an optical characterization to ascertain whether it can host persistent luminescence sources.[13] In their study, Li et al.[13] employed trivalent lanthanides as emitting centers, exploiting their extensive spectral emission range in wide-bandgap hosts. The authors demonstrated that, with the exception of La^{3+}, Lu^{3+}, and Pm^{3+}, trivalent lanthanides generate persistent luminescence spanning a range of 200–1700 nm in the following wide-bandgap hosts: $NaYF_4$, Cs_2NaYF_6, XPO_4, YBO_3 where X represents either Y, Sc, Lu, or La.[13] It is imperative to ascertain the characteristics of the forbidden electronic band of the $(Na_5(Ti_3O_3F_{11}))$/FTO/glass structure. Accordingly, the aim of the present article is to initially determine whether $(Na_5(Ti_3O_3F_{11}))$ can be classified as a wide-bandgap material, which in turn will establish its potential suitability for persistent luminescence applications.

2. Experimental Section

2.1. Materials Development

The experimental technique and degreasing method utilized in the present study are comparable to those previously documented in the literature.[8,12] Two types of samples were synthesized using high-purity starting materials, including ammonium hexafluorotitanate (99.99%), boric acid (98%), NaCl, and F:SnO_2-coated glass substrates (FTO), resulting in the formation of pentasodium trioxoundecafluoro-trititanate structures both on FTO substrates and in powder form. Substrate cleaning technique: the substrates, as received, underwent a multistep cleaning process, involving successive treatments with hot trichloroethylene, acetone, and methanol, followed by rinsing with deionized water (DI) and drying with nitrogen gas. Precursor composition: for a standard plate synthesis, a 90 mL precursor solution was prepared using DI as the solvent, comprising 0.94 M NaCl, 24 mM ammonium hexafluorotitanate, and 56 mM boric acid. The mixture was subjected to vigorous magnetic stirring until all components were fully dissolved. The resulting precursor solution was then transferred to a Teflon container and placed inside a stainless-steel autoclave at ambient temperature. Sample deposition:[9,13] 1) Plate fabrication: The cleaned FTO substrate was positioned at an angle of ≈45° against the autoclave wall, with its conductive side facing downwards, and then submerged in the precursor solution. The autoclave was subsequently sealed and heated in a preheated oven at 100 °C for a duration of 2 h;[8,12] 2) Powder formation: following the completion of experiment (1) involving the development of $Na_5(Ti_3O_3F_{11})$ on FTO, a white precipitate was observed to have formed and settled at the bottom of the Teflon container due to gravity. The precipitate was put through a sieve, while the filtered substance was washed

with distilled water to remove impurities, and then dried in a pre-heated oven at 100 °C for 15 min to yield a dry powder.

2.2. Sample Preparation

Diffuse reflectance spectroscopy (DRS) measurements were done with a Varian Cary 500 UV-Vis-NIR spectrophotometer and a Harrick Scientific Praying Mantis Diffuse Reflection Accessory at room temperature. **Figure 1** illustrates the samples that underwent DRS characterization, as detailed in this article. The DRS measurements were conducted on the glass substrate, which was uncoated with fluorine-doped tin oxide (FTO) (see Figure 1a). Moreover, the glass substrate coated with fluorine-doped SnO_2 (Figure 1b), $Na_5(Ti_3O_3F_{11})$ plates grown on FTO (Figure 1c), and $Na_5(Ti_3O_3F_{11})$ in powder form (Figure 1d) were also subjected to the DRS investigation. Samples 1–3 (as illustrated in Figure 1a–c) were positioned within a suitable sample holder, which forms part of the Varian Cary 500 UV-Vis-NIR spectrophotometer and a Harrick Scientific Praying Mantis diffuse reflectance accessory. The latter is intended for use with non-powder samples, namely films. In each case, the surfaces of the non-powder samples that had not been contaminated were exposed to incident light. In addition, to perform optical characterization of the powders by DRS, the $Na_5(Ti_3O_3F_{11})$ powder was gradually loaded and pressed into a DRS powder sample holder, which was then placed in the measuring apparatus for characterization. A high-quality front-silvered mirror with a protective coating was used as a reference material for calibration to compensate for throughput variations. The reference material was implemented as a relative standard allowing for comparison between samples measured on the same instrument. It was of utmost importance that the powder adopts and maintains a cylindrical shape with an average height between 1 and 3 nm throughout the experiment–replicating the shape of the sample holder hole. In fact, Bock et al.[5] demonstrated that this protocol preserves the shape of the powder while minimizing the risk of damaging the DRS sample, such as by breaking or scratching it. Furthermore, the authors elucidated that a vast majority of powdery materials, made of particulates of a diameter of less than 1 µm, can be compressed into pellet-like structures, which are expected to function as Lambertian scatterers upon incident light illumination, while simultaneously limiting the transmission of light through it.[5]

Raman spectra were measured using a Horiba LabRAM HR Raman spectrometer with an Olympus BX41 microscope attachment. The excitation wavelength was a 514.5 nm line from a Lexel 95-SHG argon ion laser. The incident beam was focused onto the sample using a 50x LWD objective (N.A. = 0.55). The excitation Raman laser spot was 1 µm in diameter. No further preparation was necessary for the sample subjected to Raman spectroscopy analysis. Morphological characterization of the samples was done using a JEOL JSM-7001F field emission scanning electron microscope (SEM), and a JEOL ARM 200F aberration corrected transmission electron microscope (TEM) operated at 200 kV.

3. Results and Discussion

Figure 2a shows a comparison of a typical normalized Raman spectrum observed from one of the $Na_5(Ti_3O_3F_{11})$ samples developed on FTO/glass (black line) with that of $Na_5(Ti_3O_3F_{11})$ in powder form (red line). In terms of the Raman shift positions, there is a very good match between the two spectra. Figure 2b shows Raman spectra of $Na_5(Ti_3O_3F_{11})$ powder in 2D mapping. From the 2D powder Raman mapping shown in Figure 2b, it is seen the existence of the Raman shift at ≈144 cm^{-1}, originating from the powder. The position of the Raman shifts in present work corresponds with the results presented in previous reports.[8,12] In recent study,[12] while investigating the temperature dependence of Raman scattering in pentasodium trioxoundecafluorotrititanate, it was observed and discussed that several sets of crystal planes are absent in the calculated diffraction pattern of $Na_5(Ti_3O_3F_{11})$ compared to the XRD patterns of $Na_5(Ti_3O_3F_{11})$. As per ref. [12], it was concluded that the structures developed by the hydrothermal method may exhibit a different phase than that reported by Grannec et al.[14] An alternative hypothesis is that the sample has a different stoichiometry to that of $Na_5(Ti_3O_3F_{11})$ (published in ref. [8], or that it is a mixture of two materials, namely $Na_5(Ti_3O_3F_{11})$ and the compound responsible for the Raman shift observed at 144 cm^{-1}. The two samples analyzed are therefore the same material, as expected.

Figure 3 shows typical secondary electron microscopy (SEM) images at different magnifications. Figure 3a,b show micron-sized crystals in diameter with plate-like morphologies that have developed on the FTO. The structures in question have a thickness of less than one micrometer. Furthermore, they appear to be

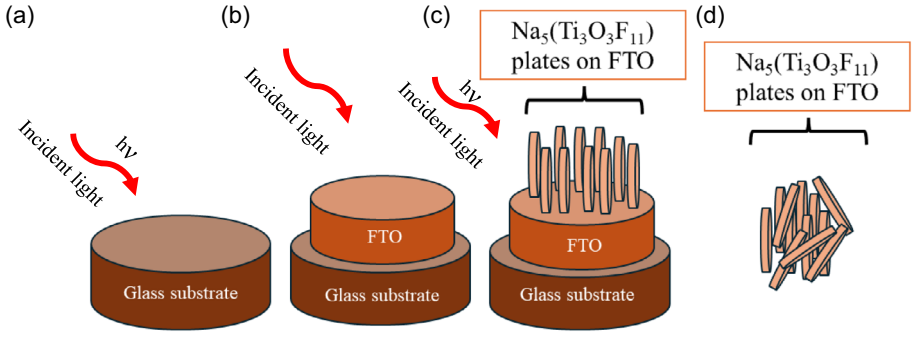

Figure 1. The following illustrations depict a) a representative glass substrate, b) a fluorine-doped SnO_2 (FTO) glass substrate, c) a $Na_5(Ti_3O_3F_{11})$ epitaxial layer grown on the fluorine-doped SnO_2 glass substrate, and d) an uncompressed $Na_5(Ti_3O_3F_{11})$ powder sample.

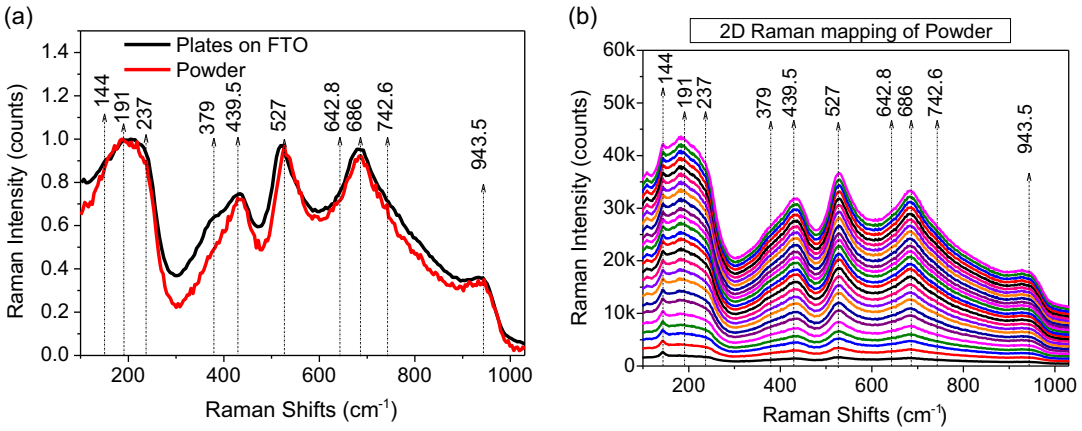

Figure 2. a) Room-temperature Raman spectra of $Na_5(Ti_3O_3F_{11})$ raw plates on FTO compared with those of $Na_5(Ti_3O_3F_{11})$ powder. b) Raman spectra of $Na_5(Ti_3O_3F_{11})$ powder in 2D mapping.

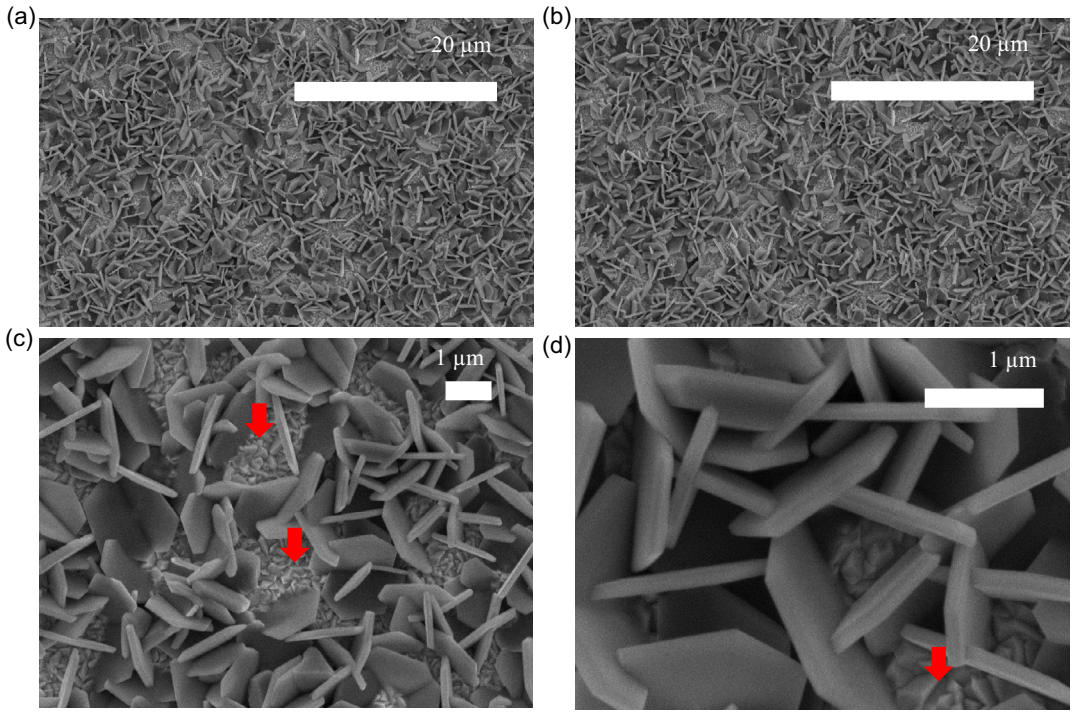

Figure 3. Typical low magnification SEM micrographs a,b) of plates developed on FTO glass by hydrothermal method. c,d) High magnification of a randomly selected section in (a).

located on the FTO. Figure 3c,d, which show enlarged views of the plates observed in Figure 3a, confirm this assertion and also reveal that these plates are hexagonal in shape. It can be reasonably accepted that the powder sample preparation procedure outlined in the experimental section will yield a DRS sample that functions as Lambertian scatterers, thereby limiting the transmission of light through the sample. We conclude that hydrothermal growth on FTO leads to the nucleation of hexagonal-shaped plates from SnO_2 (FTO). In addition, it should be noted that random pyramidal structures were also observed (not shown here). It can also be seen that the FTO/glass substrates used in this experiment have a very grainy surface (see red arrows in Figure 3c,d). For the sake of discussion, we'll refer to these structures as plates.

In order to investigate the optical properties of the materials synthesized, diffuse reflectance studies were carried out on all the two types of samples. **Figure 4** illustrates that for wavelengths greater than or equal to 300 nm, both the plates and powder exhibit transparency to visible light. This phenomenon explains the observed whiteness of the powder. As shown in the same figure, for wavelengths exceeding 300 nm, the incident light is fully absorbed by all samples. Furthermore, the absorption edge

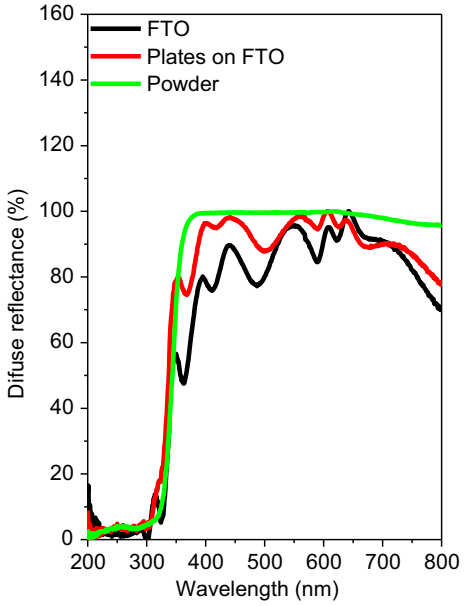

Figure 4. Normalized diffuse reflectance spectra of all samples.

of the plates is found to coincide with that of the substrate FTO (see the black spectrum in comparison with the green and red spectra). Additionally, fringes are discernible in the spectra of the FTO and plates on FTO (see black and red lines in Figure 4), which are absent in the spectrum of the powder within the wavelength range of 350–700 nm. These fringes can be attributed to the highly textured SnO_2 surface with grain-like structures, as indicated by the arrows in Figure 3c,d making the $Na_5(Ti_3O_3F_{11})$/FTO/glass system not a suitable DRS sample as per the requirements set forth in ref. [5]. From Figure 4, it can be inferred that the wavelength corresponding to the bandgap energy (E_g) of the materials deposited on FTO, or the absorption edge, is likely to fall between ≈300 and 360 nm.

A general reminder is that the absorption coefficient α and scattering coefficient s of semiconducting (or insulating) materials are dependent upon the energy $E = h\nu$ of the incident photons. Prior to determining the bandgap from DRS data, it is first necessary to review the work of Landi et al.[15] and Makula et al.[16] on determining bandgap energies from diffuse reflectance spectroscopic data. As elucidated by Landi et al.[15] the absorption coefficient α and the scattering coefficient s are intrinsic optical properties of materials, as detailed in the report "Use and Misuse of the Kubelka–Munk Function to Obtain the Band Gap Energy from Diffuse Reflectance Measurements." They represent the probabilities that light will be absorbed, scattered, or both, per unit path length. In accordance with the aforementioned authors, if the characteristic scale of inhomogeneities is $d \ll \lambda$, the scattering coefficient s is proportional to E^4; otherwise ($d \gg \lambda$), s is proportional to E^2. Furthermore, the absorption coefficients $\alpha(E)$ can be expressed as follows[17,18]

$$\alpha(E) \propto \frac{(E - E_g)^p}{E} \tag{1}$$

The parameter p in Equation (1) can be equal to 1/2, 2, 3/2, or 3 depending on the nature of interband transitions.[17,18]

The precise determination of the bandgap from diffuse reflectance spectroscopic data necessitates the meticulous application of Kubelka and Munk's model.[15,19] In order to apply Kubelka and Munk's theory, it is necessary that the system under study consist of a substrate covered with a specific material. Specifically, the system must be approximated as a cylinder with an area A and a length L, such that edge effects can be considered negligible.[15] The estimated thickness of the experimental sample corresponding to $L \to \infty$ is between 1 and 3 mm.[7] Firstly, assuming that the intensity of incoming light is I and the intensity of reflected light is J, the reflection factor of the system is defined as follows

$$R = J/I \tag{2}$$

Secondly, if we consider a sample resembling a semi-infinite cylinder ($L \to \infty$, the theory of Kubelka and Munk defines the Kubelka–Munk function as follows[20,21]

$$F(R) = K/S = (1 - R)^2/2R \tag{3}$$

where K and S are Kubelka and Munk's absorption and scattering coefficients, respectively. Moreover, as indicated in ref. [19], the values of K and S are dependent upon the intrinsic absorption coefficient α and the scattering coefficient s of the material as

$$\frac{\alpha}{s} \propto \frac{K}{S} \tag{4}$$

Thus, by combining Equation (1)–(4) and considering the power-law dependence of the diffusion coefficient on energy discussed earlier, we can express $F(R)$ as follows:[17]

$$F(R) \propto \frac{((E - E_g)^p/E)}{E^q} \tag{5}$$

It is possible to disregard the term "E^q" in Equation (7) in the vicinity of E_g. Indeed, in the vicinity of the absorption edge (around E_g), the phenomenon of light scattering can be considered negligible. Thus, Equation (5) becomes,[21]

$$(F(R) \times E)^{1/p} = A(E - E_g) \tag{6}$$

As illustrated in Equation (6), the term $(F(R) \times E)^{1/p}$. can be plotted as a function of $E - E_g$ (eV). By means of extrapolation, the value of E_g can then be obtained from the plot of $(F(R) \times E)^{1/p}$ versus $E - E_g$ (eV). This plot is generally referred to as the Tauc plot.[22,23] This approach is employed in the analysis of DRS spectra of plates, provided that the plates do not exhibit significant absorption of sub-bandgap energy. However, in the event that the plates exhibit a considerable degree of absorption of photons with energies below the bandgap E_g, the modified Kubelka–Munk method proposed by Makula et al.[16] is applied. More precisely, another linear adjustment (to be used as an abscissa) is introduced for the slope below the fundamental absorption edge (where the sub-band deviation absorptions took place). The intersection of the two fitting lines gives the estimated energy of the bandgap E_g.[16] In fact, according Makula et al.[16] the Kubelka–Munk function becomes $F(R) = F_p(R) + F_m(R)$ where $F_p(R)$ and $F_m(R)$ represent the Kubelka–Munk functions for

the plates and the sub-bandgap absorption sources, respectively. Consequently, Equation (6) takes the following forms

$$((F_p(R) + F_m(R)) \times E)^{1/p} = A(E - E_g) \quad (7)$$

Makula et al.[16] demonstrated that a more careful examination of the expansion of the square of the sum in Equation (7) (not shown here) and of the Taylor series expansion of the square root of the sum in Equation (8) (not shown here), shows that the terms with $F_m(R)$ cannot be disregarded or eliminated when $E = h\nu \rightarrow E_g$ (and hope to apply the traditional Tauc method), because then $F_p(R) > 0$ and $F_m(R) > 0$.[16] Consequently, the influence due to absorption sources in the sub-bandgap region (if any) in the plates cannot be neglected. The graphical equivalent of this is to use $F_m(R)$ as the baseline in the sub-bandgap region of the Tauc plot.

Furthermore, Zanatta[24] revisited the methods for determining the optical bandgap of semiconductors[15,17,19,25,26] and proposed a unified methodology for determining the bandgap energy. The author put forth a novel methodology for determining the optical bandgap (E_g) based on the fit of the alpha function $\alpha(E)$ with a sigmoid-Boltzmann function. To validate the Boltzmann-related method, its performance was contrasted with the E_g values provided by the standard approaches[24] when applied to the semiconductors Si, Ge, and GaAs under the conditions of bulk, powder, and amorphous (film) forms. In contrast with the conventional methodologies for determining E, as previously discussed, this approach is free from the potential inaccuracies associated with the acquisition and processing of experimental spectra. This method will be applied solely to the DRS powder results, with the objective of cross-checking the outcomes obtained through the other methods previously

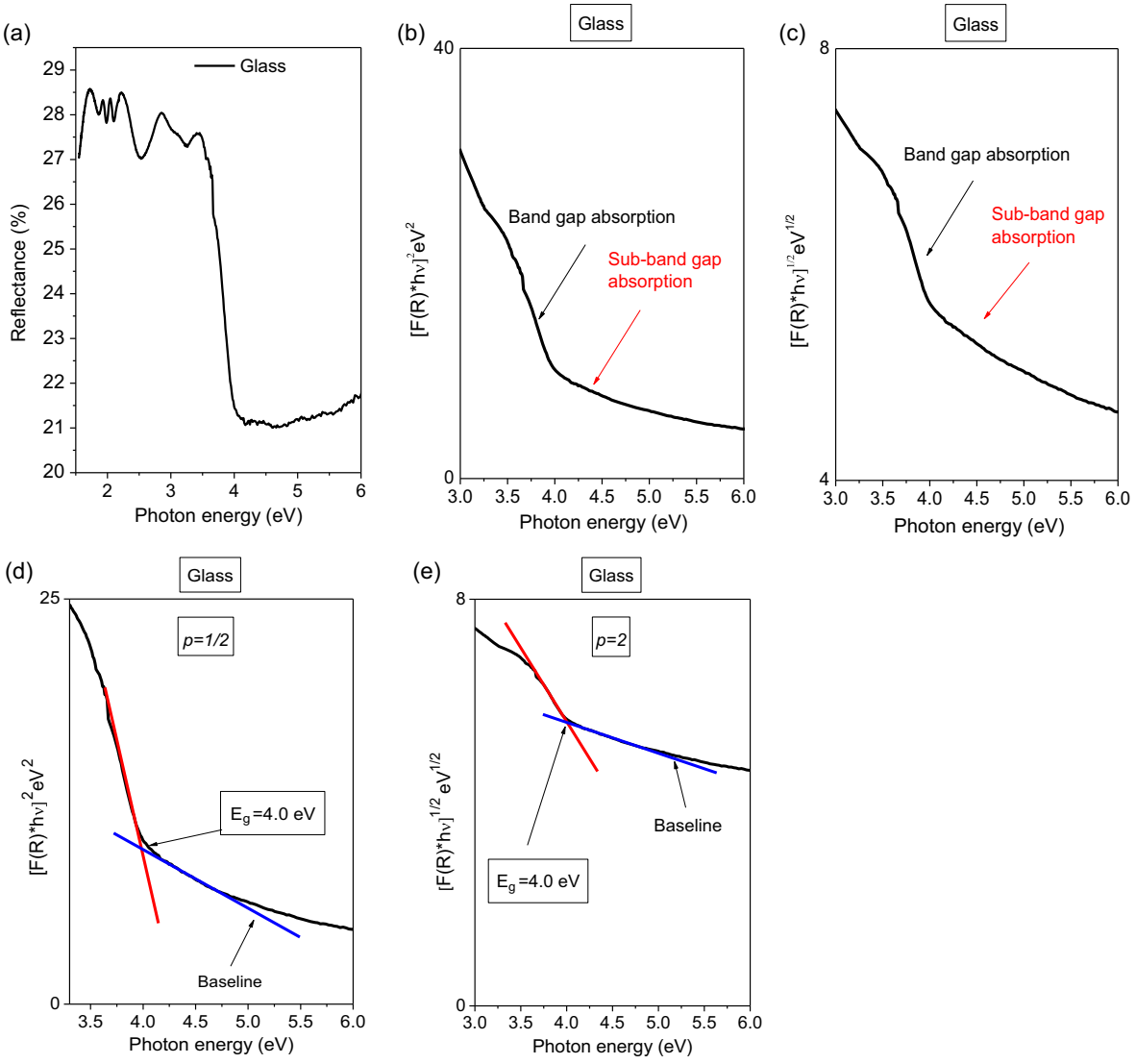

Figure 5. a) DRS of the glass substrate. b,c) Curves obtained using: Equation (8) considering (b) a direct gap (p = 1/2) and (c) an indirect gap ($p = 1/2$) showing band and sub-bandgap absorptions' contribution. d,e) The determination of the E_g is shown.

reviewed. The method entails fitting the absorption coefficients $\alpha(E)$ with the following sigmoid-Boltzmann function[24]

$$\alpha(E) = \alpha_{\max} + \frac{\alpha_{\min} - \alpha_{\max}}{1 + \exp\left(\frac{E - E_0^{\text{Boltz}}}{\delta E}\right)} \quad (8)$$

where $\alpha_{\min}$ ($\alpha_{\max}$) represents the minimum (maximum) absorption coefficient, E_0^{Boltz} denotes the energy coordinate at which the absorption coefficient is halfway between $\alpha_{\min}$ and $\alpha_{\max}$, and δE is associated with the slope of the sigmoid curve. The bandgap energy can be estimated with the following empirical relationship

$$E_g^{\text{Boltz}} = E_0^{\text{Boltz}} - n_{\text{dir-ind}}^{\text{Boltz}} \times \delta E \quad (9)$$

where $n_{\text{dir-ind}}^{\text{Boltz}}$ is the Boltzmann factors and represents two parameters ($n_{\text{dir}}^{\text{Boltz}}$ and $n_{\text{ind}}^{\text{Boltz}}$) that are to be determined as described in ref. [24].

Figure 5 shows a typical diffuse reflectance spectrum (DRS) of the glass substrate (panel a), along with Tauc plots derived from Equation (8) that consider direct ($p = 1/2$) and indirect ($p = 2$) bandgaps (panel b and c). These plots also illustrate the contribution of band and sub-bandgap absorptions. Panels d and e demonstrate the procedure for determining E_g. Figure 5b,c shows the presence of two distinct regions in the Tauc plot. The first region exhibits a linear increase in light absorption with increasing energy, which corresponds to the absorption edge (see black arrow in Figure 5b,c). The second region represents a region of sub-bandgap absorption, which is characterized by a non-flat tail (see red arrow in Figure 5b,c). Similar observations were made by Makula et al.[16] in their study of the optical properties of MO + TiO_2 and MO|TiO_2 samples. Two distinct types of samples were subjected to optical characterization. The TiO_2 was placed in direct contact with the DRS sample holder, forming the MO|TiO_2 system. A mixture of MO and TiO_2 was also prepared and characterized. The authors observed sub-band absorptions

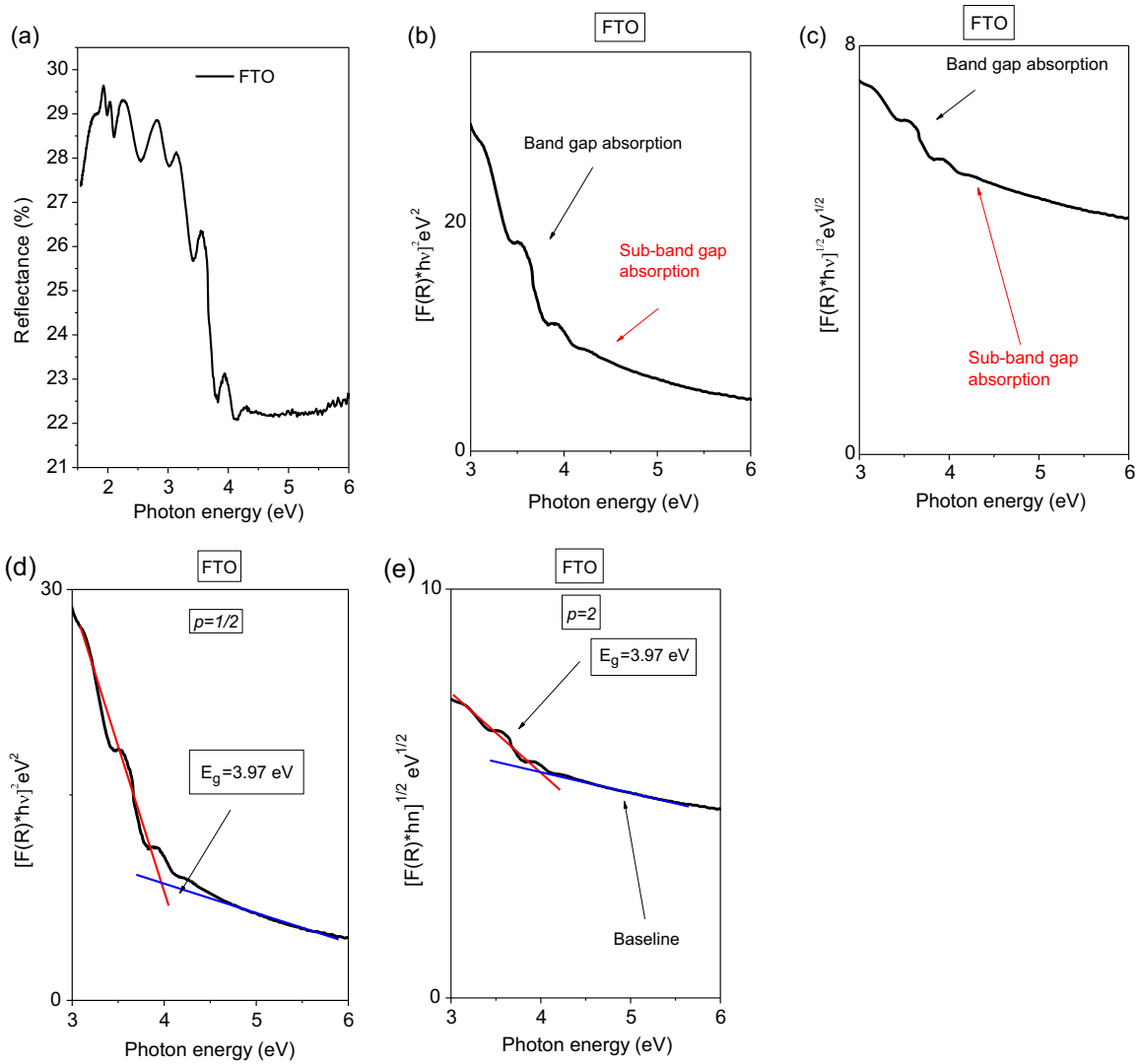

Figure 6. a) DRS of fluorine-doped tin oxide coated on glass. b,c) Curves obtained using: Equation (8) considering (b) a direct gap (p = 1/2) and (c) an indirect gap (p = 1/2) showing band and sub-bandgap absorptions' contribution. d,e) The determination of the E_g is shown.

resulting from the addition of MO to titanium dioxide and employed the aforementioned second linear fit as the abscissa to accurately determine the bandgap of titanium dioxide. Consequently, a linear fit is applied in Figure 5d,e to the initial region. Moreover, a second linear fit is employed as the abscissa for the slope below the fundamental absorption. The intersection of the two fitting lines provides an estimated value for the bandgap energy (see Figure 5d,e). The band gap energy of the typical glass substrate, as purchased, is found to be 4.0 eV when considering both the direct ($p = 1/2$) and indirect ($p = 2$) bandgaps.

Figure 6 illustrates the following: (a) the DRS spectrum of fluorine-doped tin oxide coated on glass, (b,c) Tauc diagrams based on Equation (8) considering a direct ($p = 1/2$) and indirect ($p = 2$) gap, and (d,e) the determination of E_g. The Tauc diagram (Figure 6b,c) exhibits two regions displaying a linear increase in light absorption with increasing energy, as well as a region of sub-band absorption. As shown in Figure 6d,e, the abovementioned methodology yields an energy gap of 3.97 eV for fluorine-doped tin oxide coated on glass, considering both direct ($p = 1/2$) and indirect ($p = 2$) bandgaps. As observed by Karmaoui et al.[27] an increase in the bandgap energy (E_g) was noted with an increase in the size of SnO_2 nanoparticles (NPs). The bandgap energy (E_g) for nanoparticles with a diameter of 3.4 nm ranged from 2.22 eV (indirect) to 3.12 eV (direct), while for nanoparticles with a diameter of 7.7 nm, the E_g ranged from 3.53 to 3.99 eV. Given the highly granular and textured nature of the FTO surface (see Figure 3), the observed energy bandgap of 3.97 eV is in good agreement with the reported values.

Figure 7 presents further DRS of plates grown on FTO (panel a), the corresponding Tauc diagrams based on Equation (8) considering a direct ($p = 1/2$) and indirect ($p = 2$) bandgap, which illustrate the influence of bandgap and sub-bandgap absorptions (panels b and c), and the bandgap determination (panels d and e). Figure 7b,c shows the presence of three distinct regions within the Tauc diagrams: 1) the absorption edge region; and 2) two regions of sub-band absorptions, which are likely attributable

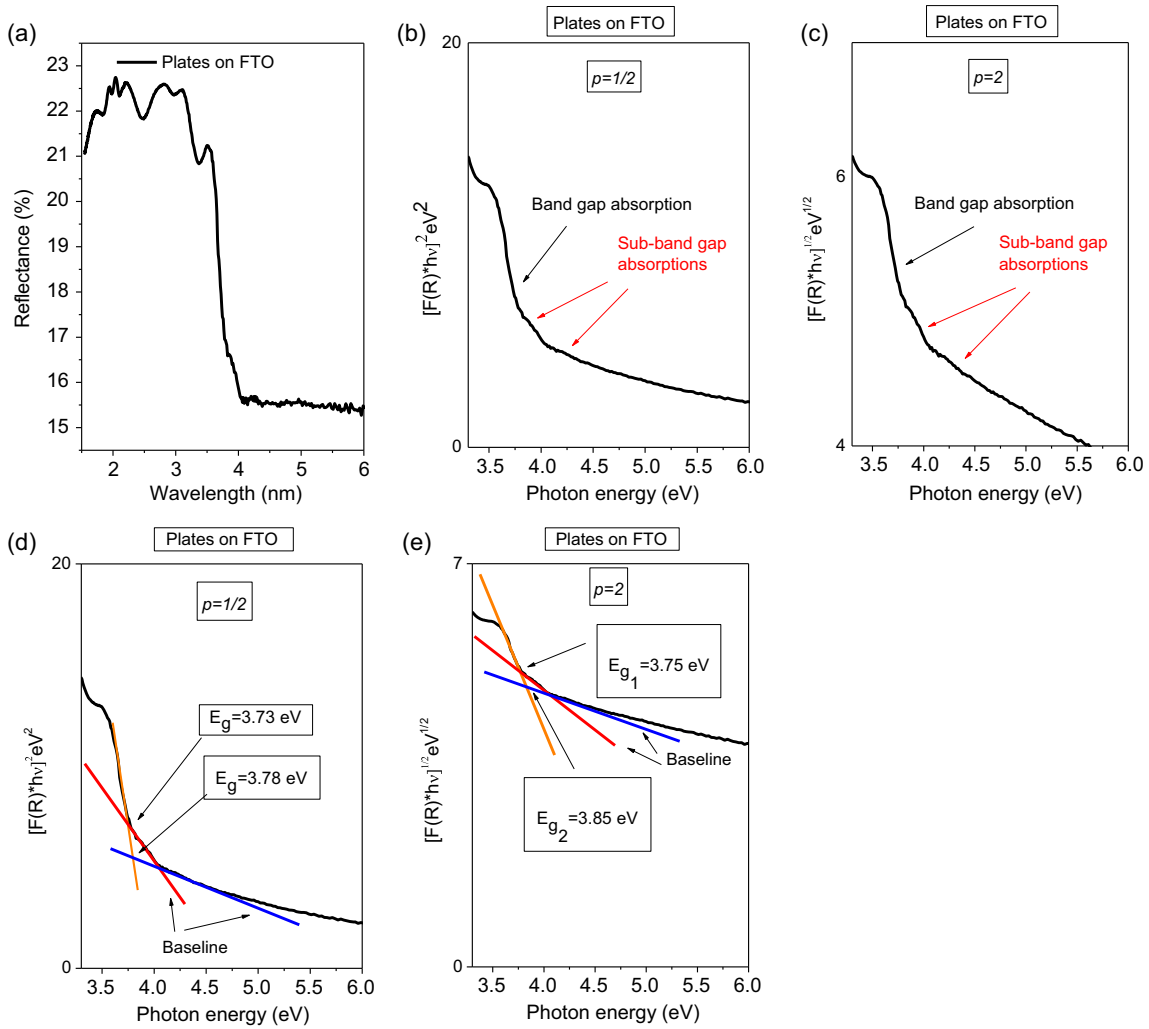

Figure 7. a) DRS of plates ($Na_5(Ti_3O_3F_{11})$) developed on fluorine-doped tin oxide coated on glass. b,c) Curves obtained using: Equation (8) considering (b) a direct gap ($p = 1/2$) and (c) an indirect gap ($p = 1/2$) showing band and sub-bandgap absorptions' contribution. d,e) The determination of the E_g is shown.

to planar defects within the plate lattice that function as recombination centers. It seems reasonable to conclude that these defects are the result of stress induced by substrate non-uniformity (see Figure 3) or lattice mismatch between FTO and $Na_5(Ti_3O_3F_{11})$, which affects the ordering of atoms (Na, Ti, F, or O) during hydrothermal plate growth, as indicated in the referenced literature.[8] Furthermore, this observation of the double sub-band absorptions prove that the plates developed on FTO don't function as Lambertian scatterers, simultaneously limiting the transmission of light through the sample. It further confirms the fact that $Na_5(Ti_3O_3F_{11})$ plates need to be prepared in pellet form as suggested by Bock et al.[5] in order to conduct accurate DRS measurements. Accordingly, in order to apply the Tauc method correctly, it is essential to consider two baselines and to undertake a comparison of the E_g values obtained for each. For purposes of discussion, we will refer to E_{g1} and E_{g2}, respectively, for the results obtained using the red and blue baselines (see Figure 7c,d). When p is equal to 1/2 (direct bandgap), the values of E_{g1} and E_{g2} are 3.9 and 3.78 eV, respectively. When $p = 2$ (indirect bandgap), the corresponding E_g values are 3.75 and 3.9 eV, respectively.

Figure 8 shows the diffuse reflectance spectra of pentasodium trioxoundecafluoro-trititanate ($Na_5(Ti_3O_3F_{11})$) in powder form. Figure 8b,c shows the corresponding Tauc diagrams based on Equation (8), considering a direct ($p = 1/2$) and indirect ($p = 2$) band gap. Figure 8d,e shows the bandgap determination. Figure 8b,d illustrate that the Tauc diagrams exhibit a single region of interest, namely the region displaying a linear increase in light absorption. This is attributed to the presence of plates, which indicate dipole-allowed transitions occurring at a direct bandgap. Moreover, the powder does not absorb light with a wavelength below the bandgap, as illustrated in Figure 8b,c. Therefore, the as prepared DRS ($Na_5(Ti_3O_3F_{11})$) powders appear to function as Lambertian scatterers, as anticipated. Moreover, the absence of

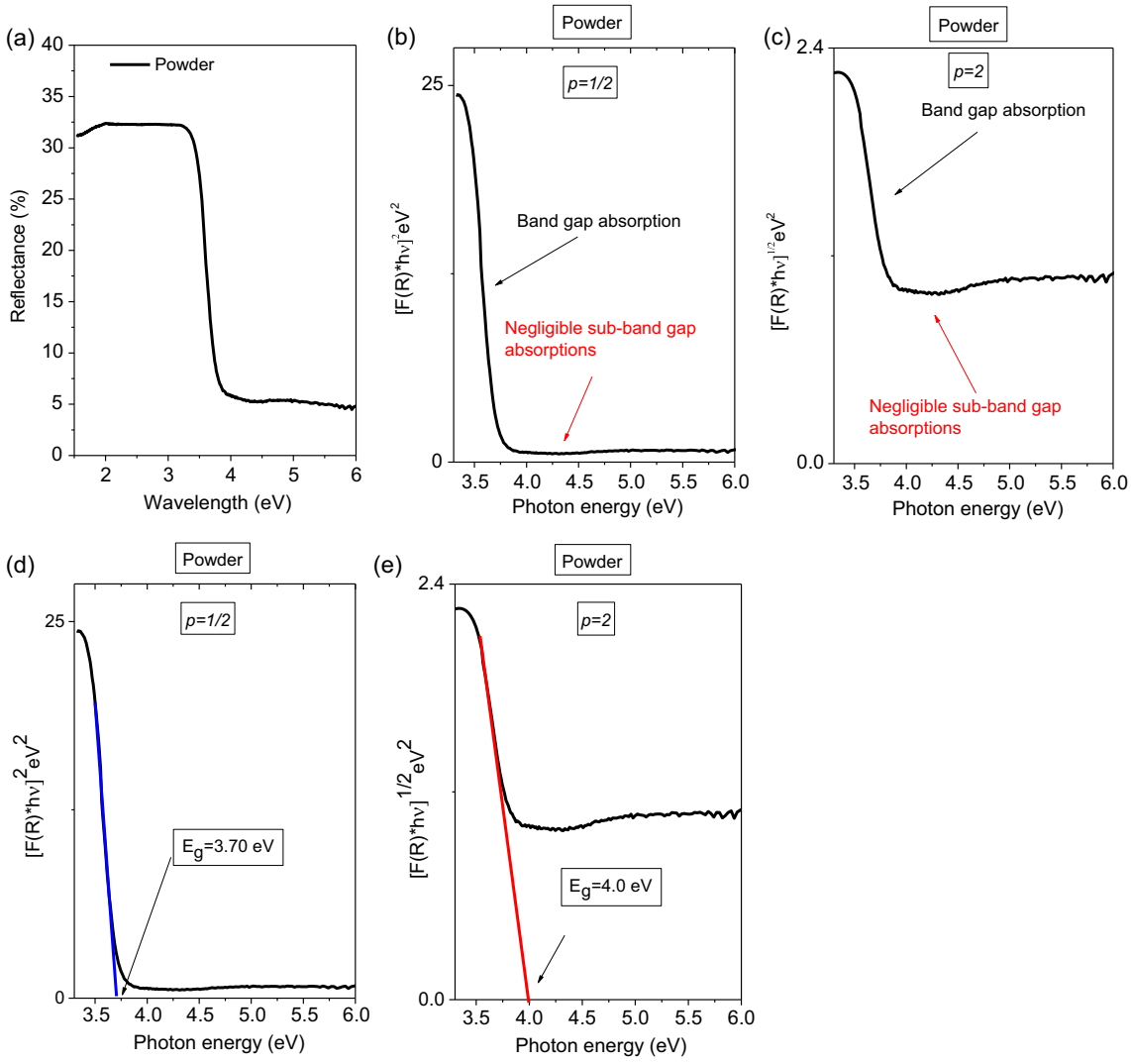

Figure 8. a) DRS of pentasodium trioxoundecafluoro-trititanate ($Na_5(Ti_3O_3F_{11})$) in powder form. b,c) Curves obtained using: Equation (8) considering (b) a direct gap ($p = 1/2$) and (c) an indirect gap ($p = 1/2$) showing band and sub-bandgap absorptions' contribution. d,e) The determination of the E_g is shown.

sub-band absorption in the DRS spectrum indicates that the hexagonal ($Na_5(Ti_3O_3F_{11})$) plates may not contain absorption centers, as discussed concerning Figure 7. In this instance, it is not necessary to establish a baseline. As illustrated in Figure 8d,e, the intersection of the x-axis of the linear fit of the Tauc plot provides an estimate of the bandgap energy. Thus, when p equals 1/2 (direct bandgap), the E_g value is 3.70 eV, and when p equals 2 (indirect bandgap), the E_g value is 4.0 eV. It is acknowledged that pentasodium trioxoundecafluoro-trititanate ($Na_5(Ti_3O_3F_{11})$) in powder form is a wide-bandgap material, with bandgap energies of $E_g = 3.70$ eV ($p = 1/2$) and $E_g = 4.0$ eV ($p = 2$).

A summary of the bandgap energies for pentasodium trioxoundecafluoro-trititanate $Na_5(Ti_3O_3F_{11})$ on FTO and in powder form, calculated from linear fits of $(F(R) \times E)^{1/p}$ versus E (Figure 6–8), among others, is given in **Table 1**. The direct band edge values of the plates developed on FTO and those of the plates in powder form appear to be in close proximity to one another. In particular, it can be seen that the direct bandgap energy of $Na_5(Ti_3O_3F_{11})$ is between 3.70 and 3.78 eV whereas that of the indirect bandgap energies between 3.75 and 4.0 eV. Nevertheless, Bock et al.[5] have posited that precise outcomes from DRS studies can only be attained by adhering to specific DRS powder sample preparation protocols. It has been demonstrated that for powders comprising particles of ≈1 µm, it is feasible to produce pellet-like samples through the application of low pressure to a gradually filled cylindrical powder sample

Table 1. Bandgap values for pentasodium trioxoundecafluoro-trititanate ($Na_5(Ti_3O_3F_{11})$) on FTO and in powder form.

Summary of calculated bandgap energies							
No	Sample reference	Molecular names	Bandgap energy [eV]			Reported values [eV]	
				Indirect, $p = 2$	Direct, $p = 1/2$	Indirect, $p = 2$	Direct, $p = 1/2$
1	Plates	$Na_5(Ti_3O_3F_{11})$	E_{g1}	3.75	3.73	–	–
			E_{g2}	3.85	3.78		
4	Powder	$Na_5(Ti_3O_3F_{11})$		4.0	3.70	–	–
5	FTO	$F:SnO_2$		3.97	3.97	2.22–3.12[27]	3.53–3.99[27]
6	Glass	–		4.0	4.0	–	

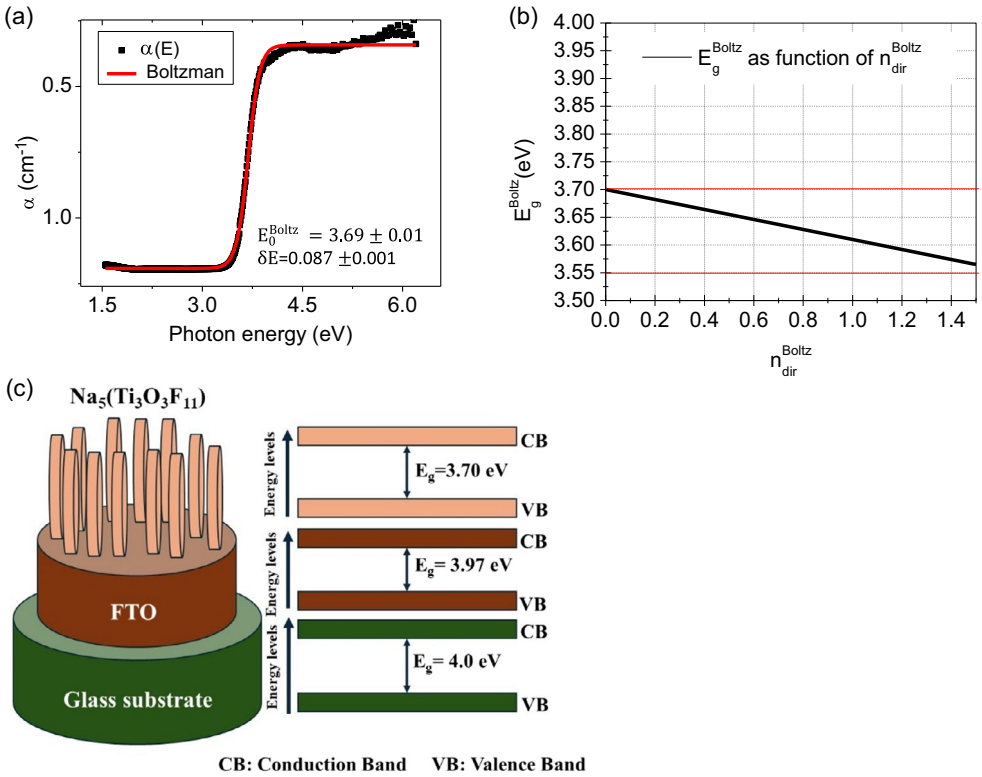

Figure 9. a) Sigmoid-Boltzmann approximation of experimental $\alpha(E)$ of the powder. The insert therein shows fitting parameters. b) Variation of E_g^{Boltz} as function of parameter n_{dir}^{Boltz}. c) Simplified energy diagram illustrating the valence (VB) and conduction (CB) bands of direct bandgap $Na_5(Ti_3O_3F_{11})$/FTO/Glass structure.

holder (a hollowed stainless-steel sample holder).[5] Hence, performing DRS analysis on as-prepared samples yields fairly accurate results. As this specific methodology was employed to obtain the data shown in Figure 8a, we can conclude–considering result obtained from the powder sample–that pentasodium trioxoundecafluoro trititanate ($Na_5(Ti_3O_3F_{11})$) is a wide-bandgap semiconductor with a bandgap energy of 3.70 eV for $p = 1/2$ (direct bandgap) and $E_g = 4.0$ eV for $p = 2$ (indirect bandgap).

Furthermore, for cross-checking purposes, **Figure 9** shows the outcomes of applying the unified methodology for estimating the bandgap of the $Na_5(Ti_3O_3F_{11})$ powder, as originally proposed by Zanatta.[24] Figure 9a shows the sigmoid-Boltzmann approximation of the experimental $\alpha(E)$ data of pentasodium trioxoundecafluoro-trititanate powder. The fitting parameters are also presented in an insert for the reader's convenience. Figure 9b-illustrates the simulation of Equation (9) utilizing the fitting parameters derived from Figure 9a. Figure 9b illustrates the variation of E_g^{Boltz}as a function of n_{dir}^{Boltz} over the interval 0–1.5. It is seen that the bandgap energy of the powder falls within the range of 3.7–3.55 eV, as evidenced by the data presented in Figure 9b. In fact, following Zanatta method,[24] we found that the average Boltzmann $n_{dir}^{Boltz} = 0.1$ leading to an estimation of $E_g \leq 3.7$ eV that is fairly in agreement with the bandgap energy determined so far when $p = 1/2$. Therefore, it can be concluded that pentasodium trioxoundecafluoro-trititanate is a material with a considerable bandgap as established earlier. Figure 9c provides a summary of the results presented in a simplified energy diagram. This diagram illustrates the valence (VB) and conduction (CB) bands of the $Na_5(Ti_3O_3F_{11})$/FTO/glass structure, with consideration given to the direct bandgap. It should be noted that the diagram does not feature the situation at the junctions.

4. Conclusion

The successful application of the Kubelka–Munk model, modified Kubelka–Munk model and unified methodology for estimating the bandgap in semiconducting materials, as originally proposed by Zanatta, to the analysis of diffuse reflectance spectra for pentasodium trioxoundecafluoro-trititanate ($Na_5(Ti_3O_3F_{11})$) plates grown epitaxially on a fluorine-coated SnO2 glass substrate (FTO) and in powder form using a hydrothermal method was discussed. The methodology for interpreting the Kubelka–Munk $F(R)$ function and utilizing it for bandgap determination was discussed in detail. Following an extensive review of the literature, it was established that calculations of the bandgap energy (E_g) can be carried out by extrapolating a linear fit of the Tauc diagram to zero using the photon energy axis as the abscissa for a sample exhibiting negligible absorptions in the sub-bands. Nevertheless, should absorptions within the sub-bandgap be evident in the Tauc diagram, a linear fit of the Tauc diagram can be conducted in accordance with the aforementioned methodology. Moreover, an additional linear fit is employed as the new abscissa, replacing the photon energy axis utilized in the aforementioned method. Pentasodium trioxoundecafluoro-trititanate ($Na_5(Ti_3O_3F_{11})$) on FTO or in powder form was found to exhibit a wide bandgap, with bandgap energies of 3.70 eV ($p = 1/2$) and 4.0 eV ($p = 2$), respectively.

Acknowledgements

This work is supported by the African Laser Centre, Council for Scientific and Industrial Research (ALC-R003), and the Govan Mbeki Research and Development Centre (GMRDC) at the University of Fort Hare.

Conflict of Interest

The authors declare no conflict of interest.

Author Contributions

Crispin Munyelele Mbulanga, **Rudolph Erasmus**, **Chinedu Christian Ahia**, and **Johannes Reinhardt Botha** contributed to the study conception and design. Material preparation by **Crispin Munyelele Mbulanga**, **Chinedu Christian Ahia**, **Kevin Sadock Niyomugavyi**, and **Donate Harerimana**. Data collection was performed by **Crispin Munyelele Mbulanga**, **Chinedu Christian Ahia**, and **Rudolph Erasmus**. Data analysis was performed by **Crispin Munyelele Mbulanga**, **Rudolph Erasmus**, **Donate Harerimana**, **Chinedu Christian Ahia**, **Kevin Sadock Niyomugavyi**, **Hippolyte Nyengeri**, and **Johannes Reinhardt Botha**. Proof reading was done by **Johannes Reinhardt Botha**, **Chinedu Christian Ahia**, and **Edson Leroy Meyer**. The first draft of the manuscript was written by **Crispin Munyelele Mbulanga**, and all authors commented on previous versions of the manuscript. All authors read and approved the final manuscript.

Data Availability Statement

The data that support the findings of this study are available from the corresponding author upon reasonable request.

Keywords

diffuse reflectance spectroscopy, hydrothermal method, Kubelka–Munk function, material bandgap, pentasodium trioxoundecafluoro-trititanate, wide-bandgap material

Received: July 29, 2024
Revised: September 20, 2024
Published online: December 11, 2024

[1] E. Swietek, K. Pilarczyk, J. Derdzinska, K. Szaciłowski, W. Macyk, *Phys. Chem. Chem. Phys.* **2013**, *15*, 14256.
[2] I. H. Dara, A. Ankara, G. Akovali, S. Suzer, *J. Appl. Polym. Sci.* **2005**, *96*, 1222.
[3] H. Deng, J. M. Hossenlopp, *J. Phys. Chem. B* **2005**, *109*, 66.
[4] E. Spagnoli, M. Valt, A. Gaiardo, B. Fabbri, V. Guidi, *Nanomaterials* **2023**, *13*, 2708.
[5] S. Bock, C. Kijatkin, D. Berben, M. Imlau, *Appl. Sci.* **2019**, *9*, 4933.
[6] R. Alcaraz de la Osa, I. Iparragirre, D. Ortiz, J. M. Saiz, *ChemTexts* **2020**, *6*, 1.
[7] A. B. Murphy, *Sol. Energy Mater. Sol. Cells* **2007**, *91*, 1326.
[8] C. M. Mbulanga, R. Erasmus, J. E. Olivier, C. C. Ahia, E. L. Meyer, J. R. Botha, *Open Ceram.* **2021**, *8*, 100181.
[9] C. Dujardin, C. Pedrini, N. Garnier, A. N. Belsky, K. Lebbou, J. M. Ko, T. Fukuda, *Opt. Mater.* **2001**, *16*, 69.
[10] S. Shionoya, W. M. Yen, *Phosphor Handbook*, CRC Press, Boca Raton, FL **1999**.
[11] A. A. Kaminskii, *Lasers Crystals*, Springer-Verlag, New York, NY **1990**.

[12] C. M. Mbulanga, R. Erasmus, C. C. Ahia, H. Nyengeri, K. S. Niyomugavyi, D. Harerimana, E. L. Meyer, J. R. Botha, *Appl. Phys. A* **2024**, *130*, 1.
[13] L. Li, T. Li, Y. Hu, C. Cai, Y. Li, X. Zhang, B. Liang, Y. Yang, J. Qui, *Light: Sci. Appl.* **2022**, *11*, 51.
[14] J. Grannec, A. Yacoubi, J. Ravez, P. Hagenmuller, *Solid State Commun.* **1987**, *62*, 407.
[15] S. Landi Jr., I. R. Segundo, E. Freitas, M. Vasilevskiy, J. Carneiro, C. J. Tavares., *Solid State Commun.* **2022**, *341*, 114573.
[16] P. Makuła, M. Pacia, W. Macyk, *J. Phys. Chem. Lett.* **2018**, *9*, 6814.
[17] M. L. Myrick, M. N. Simcock, M. Baranowski, H. Brooke, S. L. Morgan, J. N. McCutcheon, *Appl. Spectrosc. Rev.* **2011**, *46*, 140.
[18] P. K. Basu, *Theory of Optical Processes In Semiconductors*, Clarendon Press, Oxford **1997**.
[19] L. Yang, B. Kruse, S. J. Miklavcic, *J. Opt. Soc. Am.* **2004**, *A21*, 1942.
[20] P. Kubelka, F. Munk, *Z. Techn. Phys.* **1931**, *12*, 593.
[21] M. Milosevic, S. L. Berets, *Appl. Spectrosc. Rev.* **2002**, *37*, 1326.
[22] C. C. Ahia, E. L. Meyer, C. D. Umeh, *Phys. Status Solidi A* **2024**, *221*, 2300257.
[23] C. M. Mbulanga, Z. N. Urgessa, S. R. T. Djiokap, J. A. A. Engelbrecht, R. Betz, J. R. Botha, in *Fitth Conf. on Sensors, MEMS, and Electro-Optic Systems*, Skukuza, South Africa, 8–10 October 2018, Vol. *11043*, **2019**, p. 278.
[24] A. R. Zanatta, *Sci. Rep.* **2019**, *9*, 11225.
[25] E. S. Welter, S. Garg, R. Gläser, M. Goepel, *ChemPhotoChem* **2023**, *7*, 1.
[26] A. Beer, *Ann. Phys.* **1885**, *162*, 78.
[27] M. Karmaoui, A. B. Jorge, P. F. McMillan, A. E. Aliev, R. C. Pullar, J. A. Labrincha, D. M. Tobaldi, *ACS Omega* **2018**, *3*, 13227.